MODELING OF FACIES ARCHITECTURE BY MARKED POINT MODELS

ODDVAR LIA

Norwegian Computing Center
P.O.Box 114, Blindern, N-0314 Oslo, Norway

HÅKON TJELMELAND

Norwegian Computing Center and
Department of Mathematical Sciences,
Norwegian University of Science and Technology.
N-7034 Trondheim, Norway

AND

LARS EDWARD KJELLESVIK

Geomatic a/s
P.O.Box 172, N-4033 Forus, Norway

Abstract. A stochastic model based on marked point processes for facies modeling is presented. Flexibility in spatial trends for model parameters such as size, orientation, intensity, shape etc have been a key issue in the creation of the model. Complex conditioning with many wells penetrating the same object is handled by combining the marked point objects or facies objects with Gaussian fields for the top and bottom surfaces of the individual objects. The stochastic model is described in the first part while examples illustrating the model and application is emphasized in the last part of this paper.

1. Introduction

Facies modeling is an important step in the process of building a geological model of a reservoir. Many different methods have been developed for stochastic facies modeling using marked point processes. Fluvial facies models are described in (Egeland, Georgsen, Knarud & Omre 1993), (Georgsen & Omre 1993). Shale models are described in (Haldorsen & Lake 1984) and (Syversveen & Omre 1994). Sequence stratigraphic surfaces are modeled in (Hektoen, Holden, Skare & MacDonald 1994) using marked point processes for incised valleys. Ideas from the paper by Syversveen and Omre have been important in the model which is presented here. The method for conditioning on well observations is based on that publication. More general background literature on marked point process models for geometric objects can be found in (Stoyan, Kendall & Mecke 1987), and background for the simulation algorithm can be found in (Hastings 1970), (Omre & Halvorsen 1989),(Omre, Sølna & Tjelmeland 1993).

This paper describes a rather general marked point model for facies architecture. The intention of this model was to have a great flexibility in modeling trends in intensity, size, shape as well as being able to condition on complex well observations where more than one well can penetrate the same facies object. Flexibility in the choice of shapes of the facies objects was also important. The typical prototype of a reservoir zone that can be modeled by point processes is a reservoir zone with a dominating facies that fills up most of the volume but contains bounded objects of other facies. An example can be shales or calcite sheets within a sand matrix. The first part of this paper will describe the model and the simulation algorithm while the last part will demonstrate by examples how to use this model in stochastic facies modeling.

2. Model

A marked point process can be used in facies modeling to distribute objects of different facies within a background of some other facies like for instance a sand matrix. It is characterized by the distribution of the objects in space, and how their size, shape, orientation etc varies with position. The available data for facies modeling is well observations interpreted from cores and well logs, analog data from outcrops, data from similar fields and possibly some trend information from seismic. The other input to the model is model parameters and uncertainties in these. Typically the model parameters are

Norwegian Computing Center, Box 114 Blindern, N-0314 Oslo, Norway, Tel.: (+47) 22 85 25 00

specified as spatial trends in this model and must be based very much on general geological knowledge.

The probability distribution for the model we are discussing in this paper has outcome or realizations that can be written as $u = \{u_1, u_2, \cdots, u_n\}$ where n is the total number of objects and u_i is the marked point defining a single geometric facies object. The number of objects of each facies f adds up to n. n is stochastic and determined by the intensity distribution, interaction and other restrictions included in the model.

2.1. PARAMETERIZATION OF THE INDIVIDUAL OBJECTS

Each individual object $u_i = (\boldsymbol{r}_i, s_i, \theta_i, q_i, f_i)$ is characterized by its marks which are reference position $\boldsymbol{r}$, size $s_i = (l_i, w_i, h_i)$, orientation $\theta_i = (\alpha_i, \beta_i)$, facies type f_i with associated geometric shape and Gaussian fields $T(\boldsymbol{r}'), B(\boldsymbol{r}')$ for top and bottom surface of the object. The point $\boldsymbol{r}' = (x', y', 0)$ is specified in a local coordinate system for the object defined by origin in $\boldsymbol{r}$ and the orientation angles α, β for rotation and dip. The top $T(\boldsymbol{r}')$ and bottom $B(\boldsymbol{r}')$ of the object in this coordinate system is defined by $T(\boldsymbol{r}') = -0.5(f(\boldsymbol{r}')h_i + R_i^h(\boldsymbol{r}')) + R_i^z(\boldsymbol{r}')$ and $B(\boldsymbol{r}') = 0.5(f(\boldsymbol{r}')h_i + R_i^h(\boldsymbol{r}')) + R_i^z(\boldsymbol{r}')$. Here $f(\boldsymbol{r}')$ is a userdefined prototype shape thickness associated with the facies type and $R_i^h(\boldsymbol{r}'), R_i^z(\boldsymbol{r}')$ are residual Gaussian fields for thickness and vertical position in the local coordinate system of the object. q_i represents the marks $\sigma_i^h, \sigma_i^z, T(\boldsymbol{r}'), B(\boldsymbol{r}')$ where σ_i^h, σ_i^z are the standard deviations for $R_i^h(\boldsymbol{r}')$ and $R_i^z(\boldsymbol{r}')$ respectively. See figure 1 illustrating the marks.

2.2. PROBABILITY DISTRIBUTION AND MODEL PARAMETERS

The probability distribution chosen is defined by

$$\pi(u) = C \cdot \exp\left(\sum_{i=1}^{n} a_{f_i}(\boldsymbol{r}_i, s_i, \theta_i, q_i) - \sum_{i=1}^{n}\sum_{j=i+1}^{n} V_{f_i f_j}(\boldsymbol{r}_i, s_i, \theta_i, \boldsymbol{r}_j, s_j, \theta_j)\right) \cdot I_\Omega(u) \tag{1}$$

The constant C is a normalization constant. The different terms are described in the following. The main property of the model is characterized by one part describing a system of independent objects with some intensity distribution and with probability distribution for the values for size, orientation, etc. The second term describes a pairwise interaction which depends on the position and facies of each pair of objects in the current

model. The last term $I_\Omega(u)$ is an indicator function with value 0 or 1 depending on whether a global constraint on u is fulfilled or not. In our case volume fractions with specified tolerance for the different facies can be used as constraints. If the last two parts of the expression for the probability distribution are constants, the model is a spatial marked Poisson model.

The details are described as follows:

$$\begin{aligned} a_f(\boldsymbol{r}, s, \theta, q) &= \log(\lambda_f(\boldsymbol{r})) + \log\left(g_f^s(s|\boldsymbol{r})\right) + \log\left(g_f^\theta(\theta|\boldsymbol{r})\right) \\ &+ \log\left(g_f^{\sigma^z}(\sigma^z|\boldsymbol{r})\right) + \log\left(g_f^\delta(\delta|\boldsymbol{r})\right) + \log\left(g_f^{T,B}(T, B|\sigma^z, \delta, s)\right) \end{aligned}$$

where $\lambda_f(\boldsymbol{r})$ is a position dependent trend function for intensity of facies f. It describes the expected number of objects that is simulated per volume unit in position $\boldsymbol{r}$ if the model is a marked Poisson process without interaction and global constraint term. The size distribution is $g_f^s(s|\boldsymbol{r}) = N_3(\mu_s^f(\boldsymbol{r}), \sigma_s^f(\boldsymbol{r}))(l, w, h)$ which is a multi-Gaussian probability distribution for size parameters given the position of the object. It is truncated such that only positive size parameters have positive probability. The distribution for orientation $g_f^\theta(\theta|\boldsymbol{r}) = N_2(\mu_\theta^f(\boldsymbol{r}), \sigma_\theta^f(\boldsymbol{r}))(\alpha, \beta)$ is a bi-Gaussian probability distribution for the orientation parameters given the position of the object. The distribution $g_f^{\sigma^z}(\sigma^z|\boldsymbol{r}) = N(\mu_{\sigma^z}^f(\boldsymbol{r}), \sigma_{\sigma^z}^f(\boldsymbol{r}))(\sigma^z)$ is a Gaussian probability distribution for the parameter σ^z given the position of the object while $g_f^\delta(\delta|\boldsymbol{r}) = N(\mu_\delta^f(\boldsymbol{r}), \sigma_\delta^f(\boldsymbol{r}))(\delta)$ is a Gaussian probability distribution for the parameter $\delta = \sigma^h/h$ given the position of the object. The probability distribution for the two Gaussian fields $R^h(\boldsymbol{r}')$ and $R^z(\boldsymbol{r}')$ which are added to the trend thickness and vertical position of a single object is denoted by $g_f^{T,B}(T, B|\sigma^z, \delta, s)$ as described above. The spatial correlation functions for these fields depend only on facies while the variance depends on the standard deviations σ^z and $\sigma^h = h\delta$ for the individual objects.

$V_{f_i f_j}(\cdot, \cdot, \cdot, \cdot, \cdot, \cdot)$ is defined by

$$V_{f_i,f_j}(\boldsymbol{r}_i, s_i, \theta_i, \boldsymbol{r}_j, s_j, \theta_j) = v_{f_i,f_j}(d_{f_i,f_j}(\boldsymbol{r}_i, s_i, \theta_i, \boldsymbol{r}_j, s_j, \theta_j))$$

where $d_{f,f'}(u, u')$ is a generalized distance. One example is the distance $d_{f,f'} = \sqrt{(\frac{\Delta x}{a})^2 + (\frac{\Delta y}{b})^2 + (\frac{\Delta z}{c})^2}$ between the reference points for two different objects of either the same facies ($f = f'$) or different facies ($f \neq f'$). The function $v_{f,f'}(d)$ is a positive function falling to 0 as d increases. For all pairs of objects where V_{f_i,f_j} is non-zero, this term can be thought of as a repulsion force in the model. Note that if V_{f_i,f_j} is increased, the term in equation 1 is decreased and hence the probability density.

3. Simulation algorithm

The simulation is split into two main steps. The first one simulates u^* which is the objects and their marks except for the residual Gaussian fields using a Metropolis-Hastings algorithm. The residual Gaussian fields $R^h(\boldsymbol{r}')$ and $R^z(\boldsymbol{r}')$ are simulated for all objects after the first part of the simulation is finished. This can be done since we have constructed a model such that

$$\pi(u^*, T, B|obs) = \pi(u^*|obs) \cdot \pi(T, B|u^*, obs)$$

The first part of the simulation will ensure that the observed objects are close to the correct position where wells are penetrating the objects, but they do not in general match exactly. The discrepancy is regarded as a component of the residual Gaussian fields in the observations. The second step will use conditional Gaussian simulation to condition the observed objects such that wells are penetrating the observed objects in the intervals of the wells where they are observed. This approach has the advantage that many wells can penetrate the same object because of the degree of freedom introduced by the Gaussian fields. It is also much faster than a simulation from a model where the Gaussian fields have to be simulated simultaneously with the other marks in the Metropolis-Hastings loop. To be able to condition on the global constraints I_Ω, a simulated annealing term $\exp\left(-\frac{V(u,\Omega)}{T(t)}\right)$ is introduced instead of I_Ω. Here $V(u,\Omega)$ is a distance function between the target for volume fraction and the simulated volume fraction at a certain iteration number t. $T(t)$ is the annealing schedule and a function decreasing toward 0 as t increases. The model we are simulating from is denoted $\pi_{T(t)}(u)$ in the following and here $T(t)$ should approach 0 in order to get $\pi(u)$ which is our probability density function.

The main simulation loop for the first part of the simulation can briefly be described as follows:

1. Set $t = 0$ and define an initial start realization u_0 which is consistent with the well observations but not necessarily with the global constraints. If we denote $o_i = \{o_i^1, o_i^2, \cdots, o_i^{w_i}\}$ as the group of w_i observations belonging to the same observed object u_i, we are in fact simulating from the conditioned distribution $\pi(u|\{o_i\}_{i=1}^m)$ where m different groups of observations are determined during the initialization algorithm. Each group o_i corresponds to observations of the same object.

2. Draw a potential new realization u'_{t+1} from a probability distribution or transition kernel $Q(u'_{t+1}|u_t)$. In our model it is constructed to be one of the following transitions:
   (a) Remove one of the unobserved objects from u_t selecting the object uniformly among the existing unobserved objects.
   (b) Add a new unobserved object by drawing a position, facies type and then the other marks from $g_f^s(s|\boldsymbol{r})$, $g_f^\theta(\theta|\boldsymbol{r})$, $g_f^{\sigma^z}(\sigma^z|\boldsymbol{r})$ and $g_f^\delta(\delta|\boldsymbol{r})$.
   (c) Change an existing object by a new object of the same facies and if observed also conditioned on the same observations. If the object is not observed in any wells, the change is in fact a combination (a) and (b) above. For an observed object it is not possible to draw all the marks directly from the distributions $g_f^s(s|\boldsymbol{r})$, $g_f^\theta(\theta|\boldsymbol{r})$, $g_f^{\sigma^z}(\sigma^z|\boldsymbol{r})$ and $g_f^\delta(\delta|\boldsymbol{r})$. The simulation algorithm is here chosen such that the parameters are drawn in the sequence $x, y, l, w, \alpha, \beta, z, h$. It is also checked that the correct wells are penetrating the object.
3. Compute the acceptance probability

$$\alpha(u'_{t+1}|u_t) = \min\left(1, \frac{\pi_{T(t)}(u'_{t+1})}{\pi_{T(t)}(u_t)} \cdot \frac{Q(u_t|u'_{t+1})}{Q(u'_{t+1}|u_t)}\right) \tag{2}$$

4. Accept with probability $\alpha(u'_{t+1}|u_t)$ the potential new realization. Set $u_{t+1} = u'_{t+1}$ if accepted. Otherwise set $u_{t+1} = u_t$
5. Set $t = t + 1$
6. Check that stop criteria is satisfied or start new iteration. A limit on the number of iterations or a combination of number of iterations and acceptable volume fractions is used as stop criteria.

The second part of the simulation draws the Gaussian fields for each object and sample the objects into a grid. In general experimental experience must be used to determine whether a given number of iterations is sufficient or not for convergence of the realization.

4. Some examples illustrating different model parameters

In this section we will illustrate some of the properties of the model and include examples of reservoir zones modeled using this method. The intensity or number of objects per volume unit is one characteristic of the model

described. Realizations from models with different trend functions for intensity are displayed in the figures 2, 3 and 4. Note that facies realizations from other models can be used as background facies as in the example in figure 4. For instance fine scale facies objects within fluvial channel facies can be modeled by defining high intensity within channel facies and low outside. Clustering of objects can be modeled based on an underlying realization of objects which define volume with high and low intensity as in the example in figure 3. Seismic data interpreted as relative intensity maps for some facies is useful information in specifying trend functions for intensity. Trends in size and orientation can be chosen as user defined 3D grids as well. The figures in 5 display realizations with trends in size and direction, as well as in uncertainty of size and direction. The interaction term in the probability density function in equation 1 can be used to model repulsion between the individual objects. Repulsion between objects of the same facies or between objects of different facies is possible to model. Figure 6 illustrates realizations from two different models with interaction. The model for the left plot[1] contains two facies with repulsion both between individual objects of the same facies and different facies. The range of the repulsion is smaller between objects of the same facies as between objects of different facies, hence the clustering of objects of same facies. In this example the volume fractions are specified to be equal for both facies. The model for the right plot in this figure contains one facies in addition to the background facies. Here the interaction function takes the angle of rotation of the individual objects into account such that close neighbour objects should have the same orientation while more far distant neighbours can have different angles of rotation. The trend function for the angle is here constant equal to 0 with constant standard deviation of 80 degrees.

Two composite examples which illustrates the conditioning is displayed in figure 7 as fence diagrams. The first one is a simple model for a fluvial fan with two sand types, a high and low permeable sand and shale background. The second illustrate a reservoir zone with large and small shales within a sand background. The conditioned realizations was based on 50 artificial wells taken from the unconditioned realizations and a few of those artificial

[1]For models with repulsion it is always a bit difficult to be sure that a simulation has converged or not. The examples here have run through 600.000 iterations and the number of objects are about 1000, but still it might be that the convergence is so slow that even more iterations should have been used. Probably there would be only two clusters in a converged realization and with a border line between the two clusters that have a minimum length in order to minimize the total interaction potential. The implementation is however rather fast and can run about 1000 iterations per second in the MH-loop depending on the interaction range and number of objects so it is possible to run even millions of iterations.

wells are used in the fence plots. For the fluvial fan the high permeable sand is found in the upper left corner of the cross section plots while medium permeable sand is spread out as a buffer between the high permeable sand and the background shale. Different intensity functions and different size distribution are given for the two sand facies building the fan from left to right diagonally across the simulation volume. For the shale model one can clearly see a long range variability of the depth and thickness of the large shales due to the Gaussian fields for thickness and depth. For the small shales only kriging is used because the size is relatively small but simulation of the Gaussian fields for thickness and depth can of course be used for these too.

5. Summary and conclusions

The flexibility of specifying spatially dependent probability distributions of most of the model parameters in combination with the large degree of freedom introduced by Gaussian residual fields for top and bottom of the objects has made this model easier to use in facies modeling than many other marked point process models.

Acknowledgements

Thanks to T.Svanes, K.A.Jakobsen (Statoil a/s), G.Shanor (Geomatic a/s) and A. Syversveen (Norwegian University of Science and Technology) for contribution to the model specification.

References

ECM (1994), *ECMOR IV, 4th European Conference on the Mathematics of Oil Recovery*, Røros, Norway.

Egeland, T., Georgsen, F., Knarud, R. & Omre, H. (1993), Multi facies modeling of fluvial reservoirs, *in* '68th Annual Technical Conference and Exhibition', Society of Petroleum Engineers, Houston, Texas, pp. 863–872. SPE 26502.

Georgsen, F. & Omre, H. (1993), Combining fiber processes and Gaussian random functions for modeling fluvial reservoirs, *in* Soares (1993), pp. 425–440.

Haldorsen, H. H. & Lake, L. W. (1984), 'A new approach to shale management in filed scale models', *SPE Journal* pp. 447–457.

Hastings, W. K. (1970), 'Monte Carlo sampling methods using Markov chains and their applications', *Biometrika*.

Hektoen, A., Holden, L., Skare, Ø. & MacDonald, A. (1994), Combining gaussian fields

and fiber processes for modelling of sequence stratigraphic bounding surfaces, *in* ECM (1994).

Omre, H. & Halvorsen, K. B. (1989), 'The Bayesian bridge between simple and universal kriging', *Math. Geol.* **21**(7), 767–786.

Omre, H., Sølna, K. & Tjelmeland, H. (1993), Simulation of random functions on large lattices, *in* Soares (1993), pp. 179–199.

Soares, A., ed. (1993), *Geostatistics Tróia '92*, proc. '4th Inter. Geostat. Congr.', Tróia Portugal, 1992, Kluwer Academic Publishers, Dordrecht.

Stoyan, D., Kendall, W. S. & Mecke, J. (1987), *Stochastic Geometry and its Applications*, John Wiley & Sons, New York.

Syversveen, A. & Omre, H. (1994), Marked point models with complex conditioning used for modelling shales, *in* ECM (1994). 14 pp.

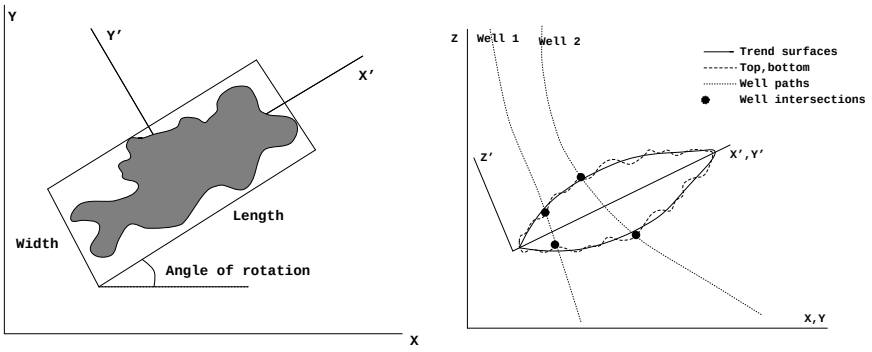

Figure 1. Illustration of the geometric parameters or marks describing an object. The length,width,rotation angle, dip and trend thickness map is illustrated in addition to the actual top, bottom and horizontal extent of an object. The local object coordinate system is indicated.

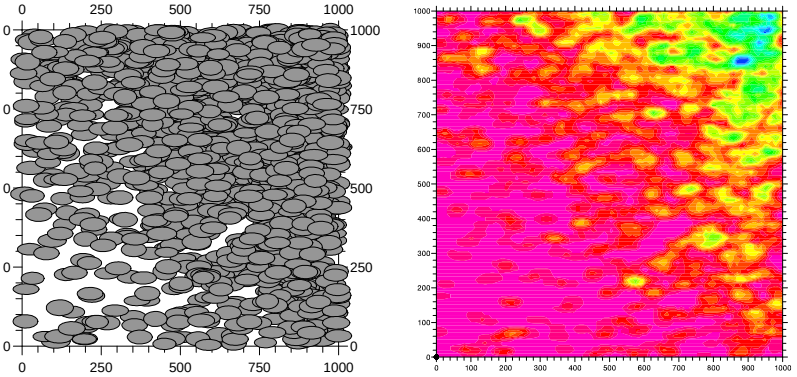

Figure 2. A realization with diagonally exponential increasing intensity. The plot is horizontal projections of parametric (not grided) realization to the left and a grided volume fraction map to the right.

Norwegian Computing Center, Box 114 Blindern, N-0314 Oslo, Norway, Tel.: (+47) 22 85 25 00

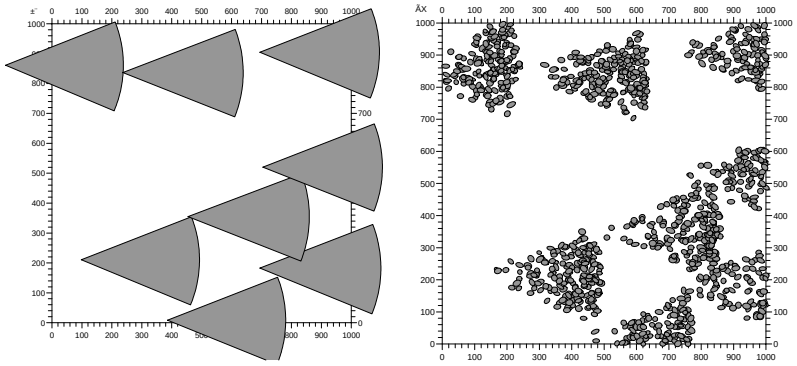

Figure 3. The left plot is a realization of underlying objects representing high intensity volumes for the objects in the realization to the right. If the left plot illustrates facies objects, they could be thought of as a kind of background facies for the objects in the right plot.

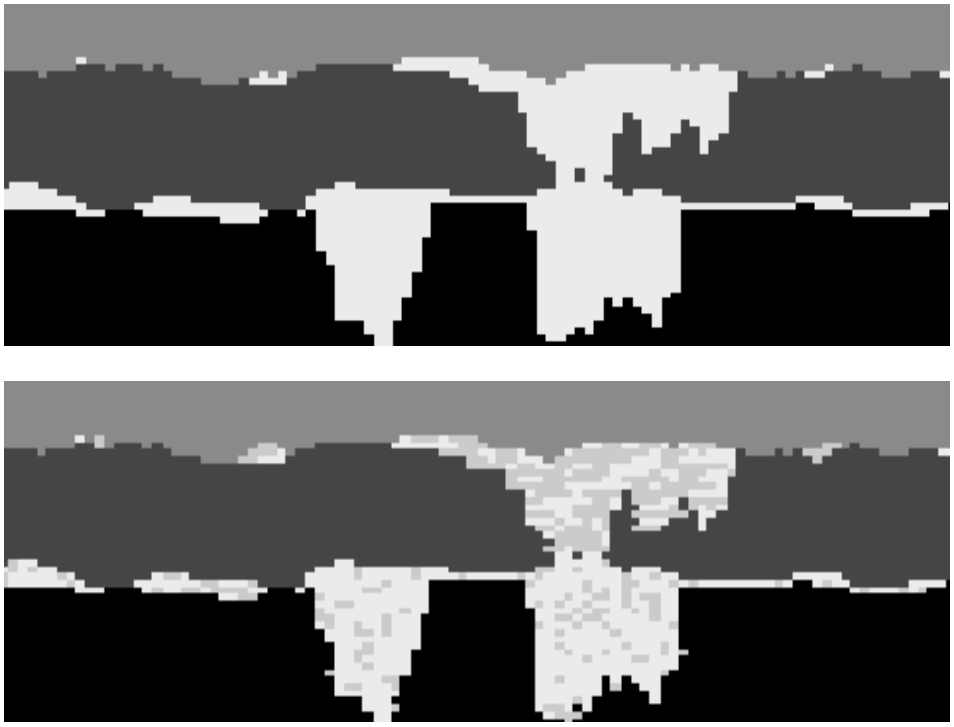

Figure 4. The uppermost plot is a cross section through sequence stratigraphic surfaces bounding different facies. The lowermost figure is the same cross section but here the sequence stratigraphic realization is merged together with a realization of small objects that have been simulated with high intensity within certain layers of the sequence stratigraphical realization.

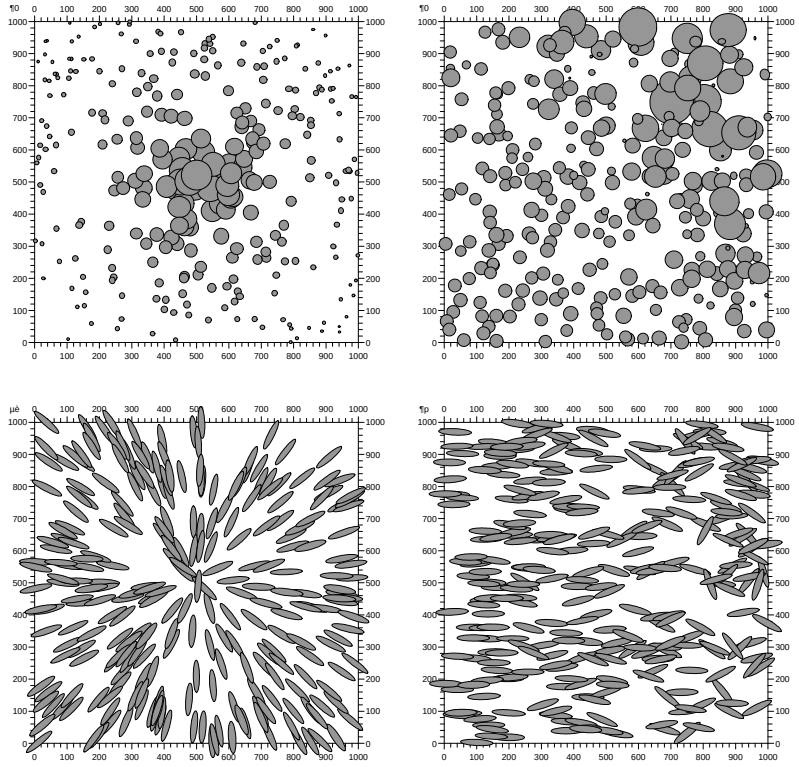

Figure 5. Realizations are displayed which illustrates models with spatially varying trend functions for expectation value and standard deviation of size and orientation.

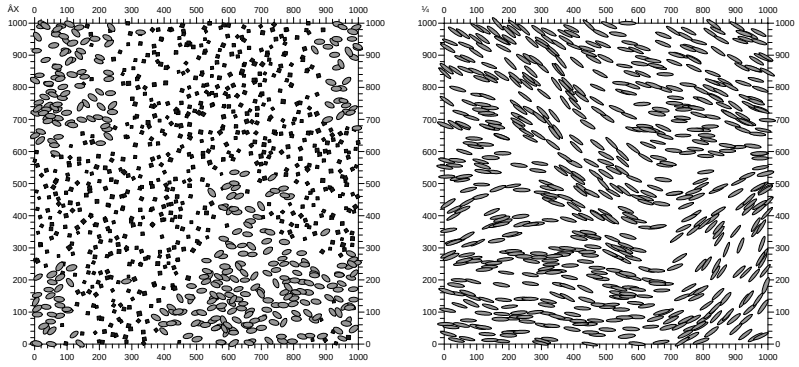

Figure 6. The realization displayed in the left figure illustrate a model with interaction both internally within the same facies and between objects of different facies.The interaction distance is largest between objects of different facies. The realization in the right plot illustrate an interaction function where the angle of horizontal rotation is included such that close neighbours are parallel.

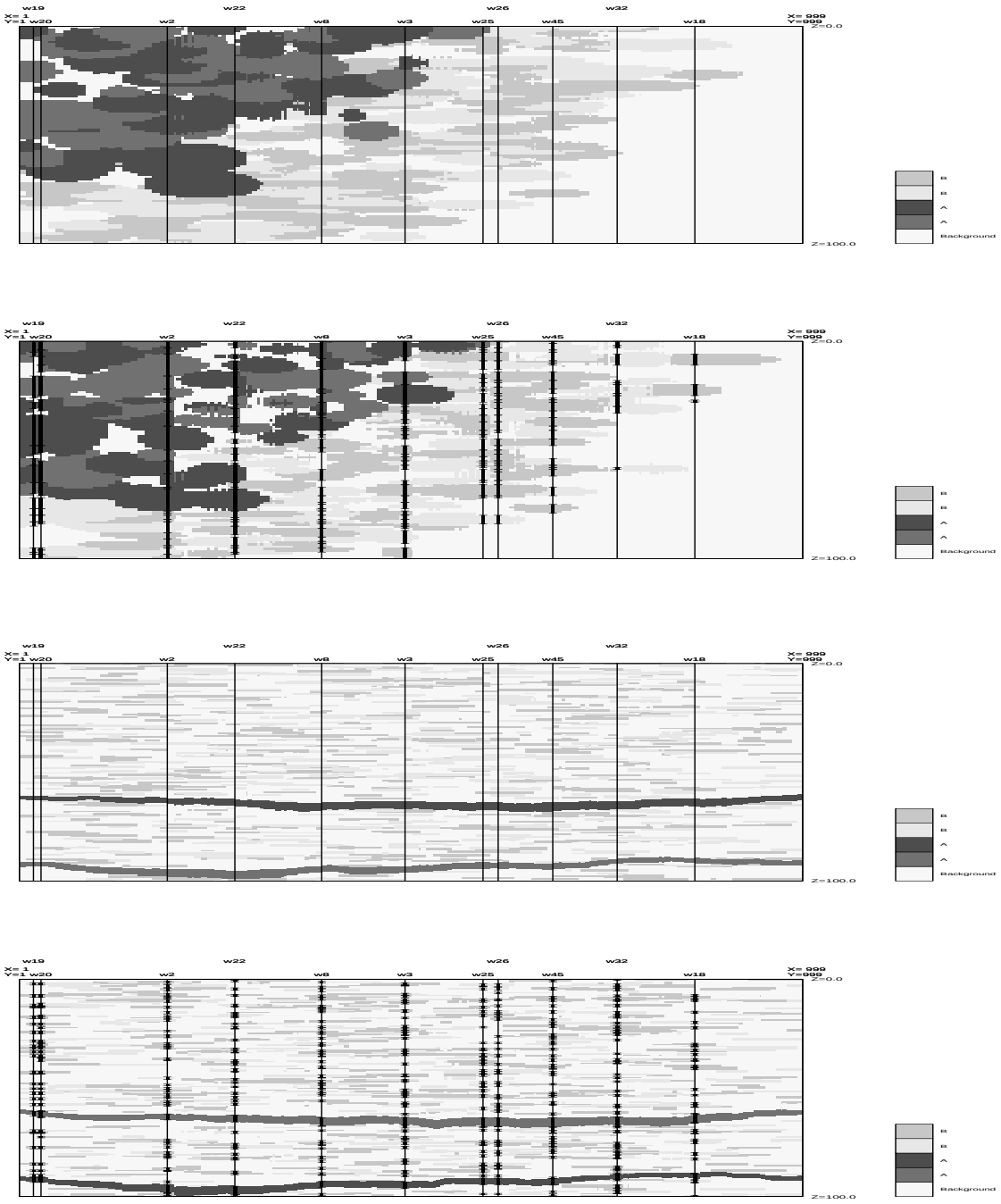

Figure 7. Realizations from two different models. The two uppermost figures are cross-section through realizations from a model with three facies, high permeable sand, medium permeable sand and background shale illustrating a fluvial fan. The first plot from the top of this figure is not conditioned on well observations but is used as the 'true' reservoir while the second plot is conditioned on artificial wells taken from the unconditioned realization. The two lowermost plots are crossection through a realizations from a model with large and small barriers and background sand. The first of these two plots is unconditional simulation while the last one is conditioned on artificial wells taken from the unconditional realization.

Norwegian Computing Center, Box 114 Blindern, N-0314 Oslo, Norway, Tel.: (+47) 22 85 25 00